

## Constraining $f(R)$ Gravity Theory Using Weak Lensing Peak Statistics from the Canada-France-Hawaii-Telescope Lensing Survey

Xiangkun Liu,<sup>1,\*</sup> Baojiu Li,<sup>2</sup> Gong-Bo Zhao,<sup>3,4</sup> Mu-Chen Chiu,<sup>5</sup> Wei Fang,<sup>5,6</sup> Chuzhong Pan,<sup>1</sup> Qiao Wang,<sup>7</sup> Wei Du,<sup>3</sup> Shuo Yuan,<sup>1</sup> Liping Fu,<sup>5</sup> and Zuhui Fan<sup>1,8</sup>

<sup>1</sup>Department of Astronomy, School of Physics, Peking University, Beijing 100871, People's Republic of China

<sup>2</sup>Institute for Computational Cosmology, Department of Physics, Durham University, South Road, Durham DH1 3LE, United Kingdom

<sup>3</sup>National Astronomical Observatories, Chinese Academy of Sciences, Beijing 100012, People's Republic of China

<sup>4</sup>Institute of Cosmology & Gravitation, University of Portsmouth, Dennis Sciama Building, Portsmouth PO1 3FX, United Kingdom

<sup>5</sup>The Shanghai Key Lab for Astrophysics, Shanghai Normal University, 100 Guilin Road, Shanghai 200234, People's Republic of China

<sup>6</sup>Department of Physics, Shanghai Normal University, 100 Guilin Road, Shanghai 200234, People's Republic of China

<sup>7</sup>Key Laboratory for Computational Astrophysics, The Partner Group of Max Planck Institute for Astrophysics, National Astronomical Observatories, Chinese Academy of Sciences, Beijing 100012, People's Republic of China

<sup>8</sup>Collaborative Innovation Center of Modern Astronomy and Space Exploration, Nanjing 210093, People's Republic of China

(Received 8 March 2016; published 27 July 2016)

In this Letter, we report the observational constraints on the Hu-Sawicki  $f(R)$  theory derived from weak lensing peak abundances, which are closely related to the mass function of massive halos. In comparison with studies using optical or x-ray clusters of galaxies, weak lensing peak analyses have the advantages of not relying on mass-baryonic observable calibrations. With observations from the Canada-France-Hawaii-Telescope Lensing Survey, our peak analyses give rise to a tight constraint on the model parameter  $|f_{R0}|$  for  $n = 1$ . The 95% C.L. is  $\log_{10}|f_{R0}| < -4.82$  given WMAP9 priors on  $(\Omega_m, A_s)$ . With Planck15 priors, the corresponding result is  $\log_{10}|f_{R0}| < -5.16$ .

DOI: 10.1103/PhysRevLett.117.051101

**Introduction.**—While both are able to explain the observed late-time accelerating expansion of the Universe [1,2], modified gravity theories (e.g., [3–5]) and dark energy models in general relativity (GR) (e.g., [6]) lead to different formation and evolution of cosmic structures (e.g., [7–18]). Observations of large-scale structures are therefore critical in scrutinizing the underlying mechanism driving the global evolution of the Universe and in revealing the fundamental law of gravity.

The  $f(R)$  theory is a representative modified gravity model, in which the integrand of the Einstein-Hilbert action is  $R + f(R)$ , where  $f(R)$  is a function of the scalar curvature  $R$  [8,19,20]. By choosing  $f(R)$  properly, such as the Hu-Sawicki model ([21], hereafter HS07), the theory can give rise to the late time cosmic acceleration without violating the gravity tests in the solar system and without affecting high redshift physics significantly. Matching the expansion history with that of the flat  $\Lambda$ CDM model with the matter density parameter  $\Omega_m$ , an extra degree of freedom is  $f_R = df/dR$ . For HS07,  $f_R \approx -n(c_1/c_2)[m^2/(-R)]^{n+1}$  (with the sign convention used in Zhao *et al.* [8]), and its current background value is  $f_{R0} \approx -n(c_1/c_2^2)[3(1 + 4\Omega_\Lambda/\Omega_m)]^{-(n+1)}$ . Here  $m^2 = H_0^2\Omega_m$  with  $H_0$  being the present Hubble constant,  $c_1/c_2 = 6\Omega_\Lambda/\Omega_m$ , and  $\Omega_\Lambda = 1 - \Omega_m$ . It satisfies the solar system tests for  $n \geq 1$  (HS07, [8]). On the other hand, cosmic structures can be affected significantly. Thus, independent observational studies of different scales are important in probing the nature of gravity (e.g., [22–25]).

On cosmological scales, there have been different observational analyses (e.g., [26–28]). Among them, studies of clusters of galaxies provide the most sensitive constraints (e.g., [7,29–33]) and reach a level of  $\log_{10}|f_{R0}| < -4.8$  (95% C.L.) [31].

Weak lensing effects (WL) are a key cosmological probe (e.g., [23,34–38]). Cosmic shear correlation analyses have been incorporated to constrain gravity theories (e.g., [39]). WL peak statistics, particularly high peaks, possess the cosmological sensitivities of both WL effects and massive clusters, and provide an important complement to shear correlation studies (e.g., [40–50]). In comparison with cluster studies that normally involve baryonic observables, WL peak analyses are advantageous because of the gravitational origin of WL effects.

In this Letter, we derive constraints on the HS07 model parameter  $|f_{R0}|$  for  $n = 1$ , for the first time, from WL peak abundances using WL data from the Canada-France-Hawaii-Telescope Lensing Survey (CFHTLenS) [51]. We perform mock tests to validate our pipeline before applying to actual data analyses.

**Observational data.**—CFHTLenS covers a total survey area of  $\sim 154 \text{ deg}^2$  from 171 individual pointings distributed in four regions [51]. We note that for cosmic shear correlation analyses, 129 pointings pass the systematic tests [52]. For the high peak abundances, our analyses find that using the full pointings does not introduce any notable bias comparing to that using the passed fields. We therefore keep the full data here. The photometric redshift is

estimated for each galaxy from five bands  $u^*g'r'i'z'$  observations [53]. The forward modeling LENSFIT pipeline is applied for the shape measurement [54]. After masking out bright stars and faulty CCD rows across the entire survey, the effective survey area is  $\sim 127 \text{ deg}^2$ . We select source galaxies with weight  $w > 0$ , FITCLASS = 0, MASK  $\leq 1$  and redshift in the range  $z = [0.2, 1.3]$  in our weak lensing analyses [54]. Such a selection results in a total number of 5 596 690 source galaxies. By taking into account their weights, the effective number of galaxies is  $\sim 4.5 \times 10^6$ , corresponding to the density  $\sim 10 \text{ arc min}^{-2}$ . By summing up the photo- $z$  probability distribution of each source galaxy, we obtain the redshift distribution for our source sample with  $p_z(z) = A(z^a + z^b)/(z^c + d)$  and  $A = 0.5514$ ,  $a = 0.7381$ ,  $b = 0.7403$ ,  $c = 6.0220$ , and  $d = 0.6426$ .

*Peak analyses.*—We perform WL peak analyses following the procedures described in detail in Liu *et al.* [50]. The steps are briefly summarized here. (1) We calculate the smoothed shear field taking into account properly the additive and multiplicative bias corrections. Then the convergence  $\kappa$  map is reconstructed for each individual  $\sim 1 \times 1 \text{ deg}^2$  field using the nonlinear Kaiser-Squires method (e.g., [55–57]). The corresponding smoothed filling-factor map is also generated from the positions and weights of source galaxies. We apply a Gaussian smoothing with  $W_{\theta_G}(\boldsymbol{\theta}) = 1/(\pi\theta_G^2) \exp(-|\boldsymbol{\theta}|^2/\theta_G^2)$  taking  $\theta_G = 1.5 \text{ arcmin}$ . (2) For each convergence map defined on  $1024 \times 1024$  pixels, we identify peaks by comparing their  $\kappa$  values with those of their nearest eight neighboring pixels. We exclude regions with the filling-factor values  $\leq 0.5$  in peak counting to suppress the mask effects [47,50], and also the outermost 50 pixels in each side of an individual map to eliminate the boundary effect. The total leftover area for peak counting is  $\sim 112 \text{ deg}^2$ . (3) We divide peaks into different bins based on their signal-to-noise ratio  $\nu = \kappa/\sigma_0$ , where  $\sigma_0$  is the average rms of the shape noise estimated by randomly rotating source galaxies to construct noise maps. For CFHTLenS and with  $\theta_G = 1.5 \text{ arcmin}$ ,  $\sigma_0 \approx 0.026$ . In this Letter, we consider only high peaks with  $\nu \geq 3$ . To avoid possible bias arising from a single bin with very few peaks and thus a large statistical fluctuation, we adopt unequal binning with comparable numbers of peaks in different bins, specifically  $\nu = [3, 3.1], (3.1, 3.25], (3.25, 3.5], (3.5, 4], (4, 6]$ . The peak counts are then denoted by  $N_i^d$  ( $i = 1, \dots, 5$ ).

To derive cosmological constraints from peak counts, we define the following  $\chi^2$  to be minimized [50]

$$\chi_{\text{peak}}^2 = dN^{(p')}(\widehat{C}^{-1})dN^{(p')}, \quad (1)$$

where  $dN^{(p')} = N^d - N^{p'}$  is the difference between the data vector  $N^d$  and the theoretical expectations of the peak counts  $N^{p'}$  for the cosmological model  $p'$ .

The covariance matrix  $C$  is estimated from bootstrap analyses using the CFHTLenS data themselves. The matrix  $\widehat{C}^{-1}$  is the scaled inverse covariance matrix with  $\widehat{C}^{-1} = (R_s - N_{\text{bin}} - 2)/(R_s - 1)(C^{-1})$ , where  $N_{\text{bin}} = 5$ , and  $R_s = 10000$  is the total number of bootstrap samples.

For  $N^{p'}$ , we use the theoretical model of Fan *et al.* ([44], hereafter F10). The model assumes that a true high peak is contributed dominantly from a single massive halo. The shape noise effects, the major contaminations to WL peak analyses using relatively shallow surveys, such as CFHTLenS, are fully accounted for. The cosmological quantities involved in F10 are the mass function and the internal density profile of dark matter halos, and the cosmological distances in the lensing efficiency factor as well as in the volume element. F10 has been tested extensively by comparing with simulations [47,48,50]. It has also been applied to derive cosmological constraints, within the framework of the  $\Lambda$ CDM model, from observed WL peaks [50].

We adopt the halo mass function given by Kopp *et al.* [58], valid for  $10^{-7} \leq |f_{R0}| \leq 10^{-4}$ . We compare its predictions with that from our  $f(R)$  simulations to be described in the next section, and find a good agreement. For the halo density profile in  $f(R)$  theory, studies have shown that it is not different significantly from that of the corresponding  $\Lambda$ CDM model for massive halos concerned in our peak analyses here (e.g., [8,15,59,60]). We therefore use the Navarro-Frenk-White density profile [61,62] with the mass-concentration (M-c) relation given by Duffy *et al.* [63]. We have checked and found that different choices of the M-c relation do not affect our constraint on  $|f_{R0}|$  significantly due to the weak degeneracy between these two parameters from current data. We should note that in both the mass function of Kopp *et al.* [58] and in our  $f(R)$  simulations and observational analyses, the  $\sigma_8$  parameter, the rms of the present linearly extrapolated density perturbations smoothed with a top-hat window function of scale  $8 \text{ h}^{-1} \text{ Mpc}$ , is defined to be the  $\Lambda$ CDM equivalent value rather than its true value in  $f(R)$  theory. Thus this  $\sigma_8$  should be regarded as a measure of the initial perturbations.

Our analyses concern high peaks that are physically related to halos with  $M \sim 10^{14} M_\odot$  and above. The baryonic effects on their mass function and overall density profiles are shown to be minimal (e.g., [64–66]). Depending on baryonic physics, the very central part of halos may be affected (e.g., [66]). However, our smoothing operation can suppress effectively the influence of detailed central profiles. We therefore do not expect significant baryonic effects on high peak abundances for the current WL data with relatively large statistical errors (e.g., [67]).

We focus on deriving constraints on  $(|f_{R0}|, \Omega_m, \sigma_8)$ , the parameters that WL effects are most sensitive to.

TABLE I. Summary of the prior information for different cases.

Parameter	Obs. (WMAP9)	Obs. (Planck15)	Mock ( <i>F5</i> & GR)
	(WMAP+ BAO + $H_0$ )	(TT,TE,EE+ LowP)	
$\Omega_m^{\text{prior}}$	$0.288 \pm 0.0093$	$0.3156 \pm 0.0091$	$0.281 \pm 0.0093$
$10^9 A_s^{\text{prior}}$	$2.427 \pm 0.079$	$2.207 \pm 0.074$	$2.372 \pm 0.079$
$k_{\text{pivot}} (\text{Mpc}^{-1})$	0.002	0.05	0.002
$\Omega_b$	0.0472	0.0492	0.046
$h$	0.6933	0.6727	0.697
$n_s$	0.971	0.9645	0.971

We employ priors on  $\Omega_m$  and the initial curvature perturbation parameter  $A_s$  from WMAP9 [68] or Planck15 [69], where  $A_s$  can be directly linked to  $\sigma_8$  (e.g., [7]). Thus, our total  $\chi^2$  is

$$\chi_{\text{tot}}^2 = \chi_{\text{peak}}^2 + \chi_{\Omega_m}^2 + \chi_{A_s}^2. \quad (2)$$

Here  $\chi_{\Omega_m}^2 = (\Omega_m - \Omega_m^{\text{prior}})^2 / \sigma_{\Omega_m^{\text{prior}}}^2$  and  $\chi_{A_s}^2 = (A_s - A_s^{\text{prior}})^2 / \sigma_{A_s^{\text{prior}}}^2$ , where  $\Omega_m^{\text{prior}}$  and  $A_s^{\text{prior}}$  are the prior central values, and  $\sigma_{\Omega_m^{\text{prior}}}$  and  $\sigma_{A_s^{\text{prior}}}$  are the corresponding 68% confidence limits. The specific priors are listed in Table I. These priors do not include the contributions from the constructed lensing potential that depends on gravity theories. On the other hand, for the small  $|f_{R0}|$  concerned here, the impacts of modified gravity on the primordial cosmic microwave background and on the late integrated Sachs-Wolfe effect are negligible (e.g., [28,70]). Thus, the priors we adopt here that are derived under  $\Lambda$ CDM are feasible and should not introduce biases to our constraints on  $|f_{R0}|$ . The other cosmological parameters, such as the baryon density  $\Omega_b$ , the Hubble constant  $h$ , and the power index of initial density perturbations  $n_s$ , are fixed to the corresponding values of WMAP9 or Planck15.

*Mock tests.*—To validate our pipeline, we generate mocks from ray-tracing simulations.

We run  $N$ -body simulations for flat  $\Lambda$ CDM under GR, and for  $f(R)$  theory with  $n = 1$  and  $|f_{R0}| = 10^{-4}$  (*F4*),  $10^{-5}$  (*F5*), and  $10^{-6}$  (*F6*), respectively. Besides  $|f_{R0}|$ , all the other cosmological parameters are the same in all simulations with  $\Omega_m = 0.281$ ,  $\Omega_\Lambda = 0.719$ ,  $\Omega_b = 0.046$ ,  $h = 0.697$ ,  $n_s = 0.971$ , and the  $\Lambda$ CDM-equivalent  $\sigma_8 = 0.819$ .

The simulations start at redshift  $z = 49$  with the initial conditions generated by MPGRAFIC [8]. The ECOSMOG [71] is used for the dynamical evolutions. The box size is  $1024 h^{-1} \text{Mpc}$  and the particle number is  $1024^3$ . We compare the halo mass function from these simulations with the predictions from Kopp *et al.* [58], and find a good agreement.

The mock WL analyses for GR, *F5*, and *F4* are done. Here, we mainly present the results for GR and *F5*. For

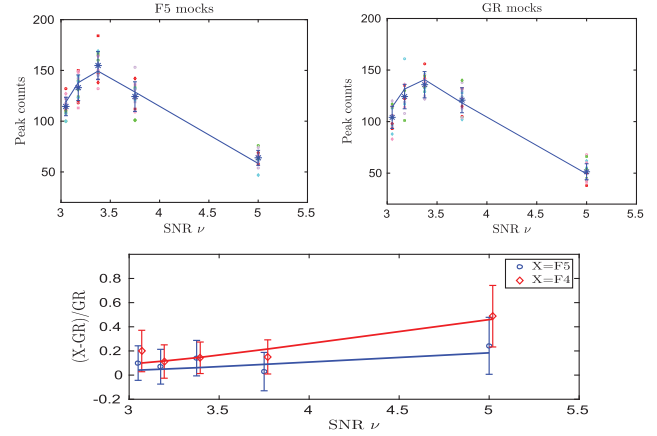


FIG. 1. Peak counts distribution from *F5* (upper left) and GR (upper right) mock simulations. Different symbols with different colors correspond to different noise realizations. The blue asterisk (\*) and the error bars are for the average values and the rms over the 15 realizations. The solid line is for our model predictions. The lower panel is for the difference ratios.

each model, we run five independent  $N$ -body simulations and pad them together to form the light cones to  $z = 3$ . The five simulations for *F5* have exactly the same initial conditions as their GR counterparts.

Based on the padded simulations, we then use 36 lens planes evenly distributed in the comoving distance to  $z = 3$  to perform multiple-plane ray-tracing calculations following closely the procedures applied in our previous studies [47,50]. To generate mock data, we divide the simulated area into different fields of  $1 \text{deg}^2$ , and match them randomly to the observational fields. In each field, we preserve the relative positions and the photo- $z$ s of the observed galaxies, as well as the masked areas. We randomly rotate source galaxies to eliminate the original WL signals, and then incorporate the reduced WL shears from ray-tracing simulations to construct the mock shear data. To better estimate the shape noise effects, we apply 15 sets of different random rotations to the source galaxies. Thus, for each model, we finally have 15 sets of mock data, each with a survey area of  $\sim 150 \text{deg}^2$ . We refer the readers to Liu *et al.* [50] for further details.

With mock data, we perform the same WL peak analyses as we do for observational data, and derive cosmological constraints to validate our analyzing pipeline.

*Results.*—We first present the results from mock simulations. Figure 1 shows the peak number distributions for *F5* (upper left) and GR (upper right). In both cases, the averaged mock results agree with our model predictions very well. The lower panel shows the difference ratios between *F5* and GR (blue) and *F4* and GR (red), respectively, which demonstrates the constraining potential of WL peak statistics on  $|f_{R0}|$ .

With these averaged data as our mock “observed” data and the covariance matrix derived by bootstrapping from

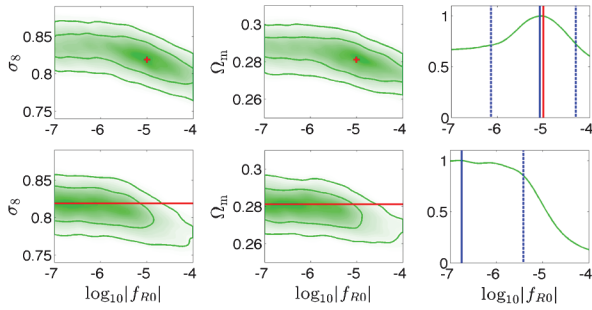


FIG. 2. Constraints derived from  $F5$  (upper) and  $GR$  (lower) mock data. In 1D distributions, blue solid and dashed lines indicate the locations of the maximum marginalized probabilities, and the corresponding 68% confidence intervals. Red solid lines and plus (+) symbols are the input parameters of the mock simulations. For the  $GR$  case,  $f_{R0} = 0$ , and we only indicate the input  $\Omega_m$  and  $\sigma_8$ .

the 15 sets of simulated catalogs, we perform Markov Chain Monte Carlo (MCMC) constraints on  $(|f_{R0}|, \Omega_m, \sigma_8)$  using COSMOMC [72] modified to include our likelihood function from WL peak abundances. As in real observational analyses, we also add the priors on  $\Omega_m$  and  $A_s$  (Table I). Here, the central value of  $\Omega_m$  is directly from the simulation input, and the  $A_s$  value is chosen to match the input  $\sigma_8$ . The  $1\sigma$  ranges for the two parameters are taken from WMAP9. For  $|f_{R0}|$ , because its value spans orders of magnitude, we sample it in log space and apply a flat prior in the range of  $\log_{10}|f_{R0}| = [-7, -4]$ .

The obtained constraints are shown in Fig. 2 for  $F5$  (upper) and  $GR$  (lower). The red symbols and lines denote the input values of the corresponding mock simulations. It is seen that the one-dimensional (1D) maximum probability values (blue solid lines) agree with the input parameters excellently. Similar results are also obtained for  $F4$  mock analyses. The flattening trend for  $\log_{10}|f_{R0}| < -6$  in the  $GR$  case is a reflection of the nondetectable differences for high peak abundances between  $GR$  and  $f(R)$  with  $|f_{R0}| < 10^{-6}$  due to the chameleon effect. The 1D marginalized constraints on  $\log_{10}|f_{R0}|$  for  $GR$  and  $F5$  mocks are shown in Table II. For  $F5$ , we show the 68% C.L. because the 95% C.L. is beyond our considered ranges of  $\log_{10}|f_{R0}|$ .

We now show the observational results from CFHTLenS. We note that in the base Planck15 constraints, a minimum neutrino mass of 0.06 eV is included in their analyses. To be consistent, we therefore also include this neutrino mass in our peak abundance calculations when the Planck15 priors are applied.

The results are presented in Fig. 3. The left panel shows the peak count distribution along with the theoretical predictions from the best-fit cosmological parameters obtained from the MCMC fittings using WMAP9 (green) and Planck15 (red) priors, respectively. The right panels show the derived constraints. The marginalized 1D

TABLE II. Constraints from mock and observational analyses.

Mock case			
Parameter	Mock case		
$\log_{10} f_{R0} $ <sup>a</sup>	GR (1D 95% limit)	$< -4.59$	
$\log_{10} f_{R0} $ <sup>a</sup>	$F5$ (1D best fit and 68% C.L.)	$-5.08^{+0.81}_{-1.06}$	
CFHTLenS			
Parameter	observation case	WMAP9	Planck15
$\log_{10} f_{R0} $ <sup>a</sup>	1D limit (95%)	$< -4.82$	$< -5.16$
$ f_{R0} $ <sup>b</sup>	1D limit (95%)	$< 7.59 \times 10^{-5}$	$< 4.63 \times 10^{-5}$
$\log_{10} f_{R0} $ <sup>c</sup>	1D limit ( $2\sigma$ )	$< -4.50$	$< -4.92$

<sup>a</sup>Probability distribution obtained based on  $\log_{10}|f_{R0}|$ .

<sup>b</sup>Probability distribution obtained based on  $|f_{R0}|$ .

<sup>c</sup> $\exp(-2)$  of the maximum probability in log space.

constraints for  $|f_{R0}|$  are shown in Table II, where the results from linear sampling on  $|f_{R0}|$  and the value whose posterior probability is  $\exp(-2)$  ( $2\sigma$ ) of the maximum probability are also listed.

It is seen that WL peak abundance analyses can provide strong constraints on  $|f_{R0}|$  even with data from surveys of an area of  $\sim 150 \text{ deg}^2$ . The 95% C.L. from log-space sampling is  $\log_{10}|f_{R0}| < -4.82$  and  $< -5.16$  with WMAP9 and Planck15 priors, respectively. The stronger constraint from Planck15 is due to its somewhat larger value of  $\Omega_m$ .

Our constraints are comparable and slightly tighter than that from Cataneo *et al.* [31] with  $\log_{10}|f_{R0}| < -4.73$  (WMAP9) and  $< -4.79$  (Planck2013) noting their wider prior of  $[-10, -2.523]$  on  $\log_{10}|f_{R0}|$ . Comparing to the results in Table 8 of Planck Collaboration 2015 XIV [28], our equivalent constraint on  $B_0$  is  $B_0 < 2.45 \times 10^{-4}$  (Planck15) (linear sampling), which is about 2–3 times

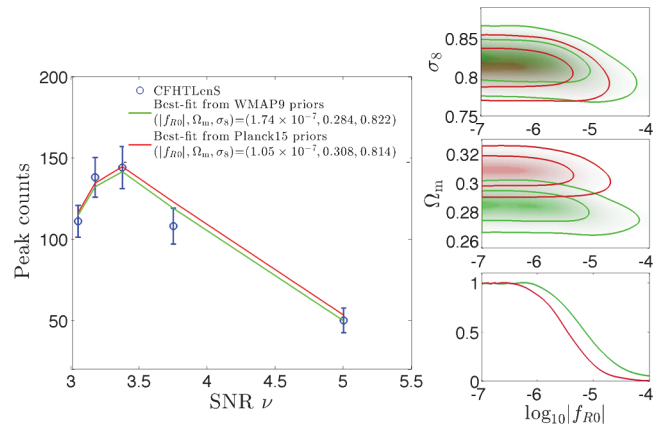


FIG. 3. Results from CFHTLenS observational data. Left: The peak counts distribution. The corresponding solid lines are the theoretical predictions with the best-fit cosmological parameters listed therein. The error bars are the square root of the diagonal terms of the covariance matrix. Right: The derived constraints. Green and red contours are the results with WMAP9 and Planck15 priors, respectively.

larger than theirs obtained by adding data of redshift space distortion and WL 2-pt correlations to Planck cosmic microwave background data.

In the analyses above, we fix  $(n_s, h, \Omega_b)$ . WL peak abundances depend on them very weakly. On the other hand, given  $A_s$ , the derived  $\sigma_8$  changes with their values, which in turn may affect our constraint on  $|f_{R0}|$ . To test this, we perform MCMC analyses by including them separately as additional free parameters and applying WMAP9 priors, which are larger than those of Planck15. We find that by adding  $n_s$  or  $h$  or  $\Omega_b$ , the constraint is weakened by  $\sim 1.4\%$ ,  $0.9\%$ , and  $0.2\%$  with  $\log_{10}|f_{R0}| < -4.75$ ,  $-4.78$ , and  $-4.81$ , respectively. Considering the negative degeneracy between  $n_s$  ( $h$ ) and  $A_s$  from WMAP9, their influences on the  $|f_{R0}|$  constraint should be even smaller.

*Summary.*—Using CFHTLenS, we derive constraints on  $f(R)$  theory, for the first time using WL peak abundance analyses. To demonstrate the potential of the probe, we focus on the specific HS07 model with  $n = 1$ . We find no evidence of deviations from GR and obtain strong limits on the  $|f_{R0}|$  parameter. For other  $n$  values with  $n > 1$ , because of the  $|f_{R0}| - n$  degeneracy (e.g., [73]), we expect that the limit on  $|f_{R0}|$  would be larger. We will perform more general studies in the future.

WL high peaks are closely associated with massive clusters, and thus the constraining power of WL high peak abundances is physically similar to that of cluster abundance studies. However, WL peak analyses are much less affected by baryonic physics than other cluster probes in which baryon-related observables are involved. On the other hand, the WL peak signal depends on the halo density profile, whose shape is determined by the concentration parameter for a Navarro-Frenk-White halo. Thus, the uncertainty in the halo M-c relation can potentially affect the cosmological constraints from WL peak abundances. This impact is weak for our current analyses given the data statistics. For future large observations, such an effect needs to be considered carefully. Our studies show that we can constrain the M-c relation simultaneously with cosmological parameters from WL peak counts to avoid potential biases from the assumed M-c relation [50].

With improved WL data, we expect that our analyses can be applied to constrain a more general class of modified gravity theories that can affect the halo abundances significantly.

This work used the DIRAC Data Centric system at Durham University, operated by the Institute for Computational Cosmology on behalf of the STFC DIRAC HPC Facility [74]. This equipment was funded by BIS National E-infrastructure Capital Grant No. ST/K00042X/1, STFC Capital Grants No. ST/H008519/1 and No. ST/K00087X/1, STFC DIRAC Operations Grant No. ST/K003267/1 and Durham University. DIRAC is part of the National E Infrastructure. The MCMC

calculations are partly done on the Laohu supercomputer at the Center of Information and Computing at National Astronomical Observatories, Chinese Academy of Sciences, funded by Ministry of Finance of People's Republic of China under Grant No. ZDYZ2008-2. The research is supported in part by NSFC of China under Grants No. 11333001, No. 11173001, and No. 11033005. L. P. F. also acknowledges the support from NSFC Grant No. 11103012, Shanghai Research Grant No. 13JC1404400 & No. 16ZR1424800 of STCSM, and from Shanghai Normal University Grant No. DY201603. G. B. Z. is supported by the 1000 Young Talents program in China. Z. H. F. and G. B. Z. are also supported by the Strategic Priority Research Program “The Emergence of Cosmological Structures” of the Chinese Academy of Sciences Grant No. XDB09000000. B. L. acknowledges the support by the U.K. STFC Consolidated Grants No. ST/L00075X/1 and No. RF040335. M. C. C. acknowledges the support from NSFC Grants No. 1143303 and No. 1143304. X. K. L. acknowledges the support from General Financial Grant from China Postdoctoral Science Foundation with Grant No. 2016M591006. To access the simulation data used in this work, please contact the authors.

\*lxk98479@pku.edu.cn

- [1] A. G. Riess *et al.*, Observational evidence from supernovae for an accelerating Universe and a cosmological constant, *Astron. J.* **116**, 1009 (1998).
- [2] S. Perlmutter *et al.*, Measurements of  $\Omega$  and  $\Lambda$  from 42 high-redshift supernovae, *Astrophys. J.* **517**, 565 (1999).
- [3] K. Koyama, The cosmological constant and dark energy in braneworlds, *Gen. Relativ. Gravit.* **40**, 421 (2008).
- [4] R. Durrer and R. Maartens, Dark energy and dark gravity: theory overview, *Gen. Relativ. Gravit.* **40**, 301 (2008).
- [5] B. Jain and J. Khoury, Cosmological tests of gravity, *Ann. Phys. (Amsterdam)* **325**, 1479 (2010).
- [6] S. Weinberg, The cosmological constant problem, *Rev. Mod. Phys.* **61**, 1 (1989).
- [7] F. Schmidt, M. Lima, H. Oyaizu, and W. Hu, Nonlinear evolution of  $f(R)$  cosmologies. III. Halo statistics, *Phys. Rev. D* **79**, 083518 (2009).
- [8] G.-B. Zhao, B. Li, and K. Koyama,  $N$ -body simulations for  $f(R)$  gravity using a self-adaptive particle-mesh code, *Phys. Rev. D* **83**, 044007 (2011).
- [9] G.-B. Zhao, B. Li, and K. Koyama, Testing Gravity Using the Environmental Dependence of Dark Matter Halos, *Phys. Rev. Lett.* **107**, 071303 (2011).
- [10] G.-B. Zhao, H. Li, E. V. Linder, K. Koyama, D. J. Bacon, and X. Zhang, Testing Einstein gravity with cosmic growth and expansion, *Phys. Rev. D* **85**, 123546 (2012).
- [11] B. Li, G.-B. Zhao, and K. Koyama, Haloes and voids in  $f(R)$  gravity, *Mon. Not. R. Astron. Soc.* **421**, 3481 (2012).
- [12] B. Li and G. Efstathiou, An extended excursion set approach to structure formation in chameleon models, *Mon. Not. R. Astron. Soc.* **421**, 1431 (2012).
- [13] B. Li, W. A. Hellwing, K. Koyama, G.-B. Zhao, E. Jennings, and C. M. Baugh, The non-linear matter and velocity power

- spectra in  $f(R)$  gravity, *Mon. Not. R. Astron. Soc.* **428**, 743 (2013).
- [14] G.-B. Zhao, Modelling the nonlinear clustering in modified gravity models. I. A fitting formula for the matter power spectrum of  $f(R)$  gravity, *Astrophys. J. Suppl. Ser.* **211**, 23 (2014).
- [15] I. Achitouv, M. Baldi, E. Puchwein, and J. Weller, Imprint of  $f(R)$  gravity on nonlinear structure formation, *Phys. Rev. D* **93**, 103522 (2016).
- [16] A. Joyce, B. Jain, J. Khoury, and M. Trodden, Beyond the cosmological standard model, *Phys. Rep.* **568**, 1 (2015).
- [17] M. C. Chiu, A. Taylor, C. Shu, and H. Tu, Cosmological perturbations and quasistatic assumption in  $f(R)$  theories, *Phys. Rev. D* **92**, 103514 (2015).
- [18] A. Stark, C. J. Miller, N. Kern, D. Gifford, G.-B. Zhao, B. Li, K. Koyama, and R. C. Nichol, Probing theories of gravity with phase space-inferred potentials of galaxy clusters, *Phys. Rev. D* **93**, 084036 (2016).
- [19] T. P. Sotiriou and V. Faraoni,  $f(R)$  theories of gravity, *Rev. Mod. Phys.* **82**, 451 (2010).
- [20] A. de Felice and S. Tsujikawa,  $f(R)$  Theories, *Living Rev. Relativ.* **13**, 3 (2010).
- [21] W. Hu and I. Sawicki, Models of  $f(R)$  cosmic acceleration that evade solar system tests, *Phys. Rev. D* **76**, 064004 (2007).
- [22] B. Jain *et al.*, Novel probes of gravity and dark energy, [arXiv:1309.5389](https://arxiv.org/abs/1309.5389).
- [23] D. H. Weinberg, M. J. Mortonson, D. J. Eisenstein, C. Hirata, A. G. Riess, and E. Rozo, Observational probes of cosmic acceleration, *Phys. Rep.* **530**, 87 (2013).
- [24] B. Jain, V. Vikram, and J. Sakstein, Astrophysical tests of modified gravity: Constraints from distance indicators in the nearby universe, *Astrophys. J.* **779**, 39 (2013).
- [25] Y. Higuchi and M. Shirasaki, The imprint of  $f(R)$  gravity on weak gravitational lensing - I. Connection between observables and large-scale structure, *Mon. Not. R. Astron. Soc.* **459**, 2762 (2016).
- [26] H. Oyaizu, M. Lima, and W. Hu, Nonlinear evolution of  $f(R)$  cosmologies. II. Power spectrum, *Phys. Rev. D* **78**, 123524 (2008).
- [27] M. Raveri, B. Hu, N. Frusciante, and A. Silvestri, Effective field theory of cosmic acceleration: Constraining dark energy with CMB data, *Phys. Rev. D* **90**, 043513 (2014).
- [28] Planck Collaboration, Planck 2015 results. XIV. Dark energy and modified gravity, [arXiv:1502.01590](https://arxiv.org/abs/1502.01590).
- [29] S. Ferraro, F. Schmidt, and W. Hu, Cluster abundance in  $f(R)$  gravity models, *Phys. Rev. D* **83**, 063503 (2011).
- [30] L. Lombriser, A. Slosar, U. Seljak, and W. Hu, Constraints on  $f(R)$  gravity from probing the large-scale structure, *Phys. Rev. D* **85**, 124038 (2012).
- [31] M. Cataneo, D. Rapetti, F. Schmidt, A. B. Mantz, S. W. Allen, D. E. Applegate, P. L. Kelly, A. von der Linden, and R. G. Morris, New constraints on  $f(R)$  gravity from clusters of galaxies, *Phys. Rev. D* **92**, 044009 (2015).
- [32] H. Wilcox *et al.*, The XMM Cluster Survey: testing chameleon gravity using the profiles of clusters, *Mon. Not. R. Astron. Soc.* **452**, 1171 (2015).
- [33] B. Li, J.-h. He, and L. Gao, Cluster gas fraction as a test of gravity, *Mon. Not. R. Astron. Soc.* **456**, 146 (2016).
- [34] M. Bartelmann and P. Schneider, Weak gravitational lensing, *Phys. Rep.* **340**, 291 (2001).
- [35] A. Albrecht *et al.*, Report of the Dark Energy Task Force, [arXiv:astro-ph/0609591](https://arxiv.org/abs/astro-ph/0609591).
- [36] LSST Dark Energy Science Collaboration, Large Synoptic Survey Telescope: Dark Energy Science Collaboration, [arXiv:1211.0310](https://arxiv.org/abs/1211.0310).
- [37] L. Amendola *et al.*, Cosmology and fundamental physics with the Euclid satellite, *Living Rev. Relativ.* **16**, 6 (2013).
- [38] L.-P. Fu and Z.-H. Fan, Probing the dark side of the Universe with weak gravitational lensing effects, *Res. Astron. Astrophys.* **14**, 1061 (2014).
- [39] J. Harnois-Déraps, D. Munshi, P. Valageas, L. van Waerbeke, P. Brax, P. Coles, and L. Rizzo, Testing modified gravity with cosmic shear, *Mon. Not. R. Astron. Soc.* **454**, 2722 (2015).
- [40] M. White, L. van Waerbeke, and J. Mackey, Completeness in weak-lensing searches for clusters, *Astrophys. J.* **575**, 640 (2002).
- [41] T. Hamana, M. Takada, and N. Yoshida, Searching for massive clusters in weak lensing surveys, *Mon. Not. R. Astron. Soc.* **350**, 893 (2004).
- [42] J. Y. Tang and Z. H. Fan, Effects of the complex mass distribution of dark matter halos on weak-lensing cluster surveys, *Astrophys. J.* **635**, 60 (2005).
- [43] J. P. Dietrich and J. Hartlap, Cosmology with the shear-peak statistics, *Mon. Not. R. Astron. Soc.* **402**, 1049 (2010).
- [44] Z. Fan, H. Shan, and J. Liu, Noisy weak-lensing convergence peak statistics near clusters of galaxies and beyond, *Astrophys. J.* **719**, 1408 (2010).
- [45] X. Yang, J. M. Kratochvil, S. Wang, E. A. Lim, Z. Haiman, and M. May, Cosmological information in weak lensing peaks, *Phys. Rev. D* **84**, 043529 (2011).
- [46] T. Hamana, M. Oguri, M. Shirasaki, and M. Sato, Scatter and bias in weak lensing selected clusters, *Mon. Not. R. Astron. Soc.* **425**, 2287 (2012).
- [47] X. Liu, Q. Wang, C. Pan, and Z. Fan, Mask effects on cosmological studies with weak-lensing peak statistics, *Astrophys. J.* **784**, 31 (2014).
- [48] C.-A. Lin and M. Kilbinger, A new model to predict weak-lensing peak counts. I. Comparison with  $N$ -body simulations, *Astron. Astrophys.* **576**, A24 (2015).
- [49] J. Liu, A. Petri, Z. Haiman, L. Hui, J. M. Kratochvil, and M. May, Cosmology constraints from the weak lensing peak counts and the power spectrum in CFHTLenS data, *Phys. Rev. D* **91**, 063507 (2015).
- [50] X. Liu, C. Pan, R. Li, H. Shan, Q. Wang, L. Fu, Z. Fan, J.-P. Kneib, A. Leauthaud, L. Van Waerbeke, M. Makler, B. Moraes, T. Erben, and A. Charbonnier, Cosmological constraints from weak lensing peak statistics with Canada–France–Hawaii Telescope Stripe 82 Survey, *Mon. Not. R. Astron. Soc.* **450**, 2888 (2015).
- [51] T. Erben *et al.*, CFHTLenS: the Canada–France–Hawaii Telescope Lensing Survey—imaging data and catalogue products, *Mon. Not. R. Astron. Soc.* **433**, 2545 (2013).
- [52] C. Heymans, L. Van Waerbeke, L. Miller, T. Erben, H. Hildebrandt, H. Hoekstra, T. D. Kitching, Y. Mellier, P. Simon, C. Bonnett, J. Coupon, L. Fu, J. Harnois Déraps, M. J. Hudson, M. Kilbinger, K. Kuijken, B. Rowe, T. Schrabback, E. Semboloni, E. van Uitert, S. Vafaei, and M. Velander, CFHTLenS: the Canada–France–Hawaii

- Telescope Lensing Survey, *Mon. Not. R. Astron. Soc.* **427**, 146 (2012).
- [53] H. Hildebrandt *et al.*, CFHTLenS: Improving the quality of photometric redshifts with precision photometry, *Mon. Not. R. Astron. Soc.* **421**, 2355 (2012).
- [54] L. Miller *et al.*, Bayesian galaxy shape measurement for weak lensing surveys—III. Application to the Canada–France–Hawaii Telescope Lensing Survey, *Mon. Not. R. Astron. Soc.* **429**, 2858 (2013).
- [55] N. Kaiser and G. Squires, Mapping the dark matter with weak gravitational lensing, *Astrophys. J.* **404**, 441 (1993).
- [56] M. Bartelmann, Cluster mass estimates from weak lensing, Cluster mass estimates from weak lensing, *Astron. Astrophys.* **303**, 643 (1995).
- [57] G. Squires and N. Kaiser, Unbiased cluster lens reconstruction, *Astrophys. J.* **473**, 65 (1996).
- [58] M. Kopp, S. A. Appleby, I. Aчитouv, and J. Weller, Spherical collapse and halo mass function in  $f(R)$  theories, *Phys. Rev. D* **88**, 084015 (2013).
- [59] L. Lombriser, K. Koyama, G.-B. Zhao, and B. Li, Chameleon  $f(R)$  gravity in the virialized cluster, *Phys. Rev. D* **85**, 124054 (2012).
- [60] D. Shi, B. Li, J. Han, L. Gao, and W. A. Hellwing, Exploring the liminality: Properties of haloes and subhaloes in borderline  $f(R)$  gravity, *Mon. Not. R. Astron. Soc.* **452**, 3179 (2015).
- [61] J. F. Navarro, C. S. Frenk, and S. D. M. White, The structure of cold dark matter halos, *Astrophys. J.* **462**, 563 (1996).
- [62] J. F. Navarro, C. S. Frenk, and S. D. M. White, A universal density profile from hierarchical clustering, *Astrophys. J.* **490**, 493 (1997).
- [63] A. R. Duffy, J. Schaye, S. T. Kay, and C. Dalla Vecchia, Dark matter halo concentrations in the Wilkinson Microwave Anisotropy Probe year 5 cosmology, *Mon. Not. R. Astron. Soc.* **390**, L64 (2008).
- [64] T. Sawala, C. S. Frenk, R. A. Crain, A. Jenkins, J. Schaye, T. Theuns, and J. Zavala, The abundance of (not just) dark matter haloes, *Mon. Not. R. Astron. Soc.* **431**, 1366 (2013).
- [65] M. Schaller, C. S. Frenk, R. G. Bower, T. Theuns, A. Jenkins, J. Schaye, R. A. Crain, M. Furlong, C. Dalla Vecchia, and I. G. McCarthy, Baryon effects on the internal structure of  $\Lambda$ CDM haloes in the EAGLE simulations, *Mon. Not. R. Astron. Soc.* **451**, 1247 (2015).
- [66] M. Schaller, C. S. Frenk, R. G. Bower, T. Theuns, J. Trayford, R. A. Crain, M. Furlong, J. Schaye, C. Dalla Vecchia, and I. G. McCarthy, The effect of baryons on the inner density profiles of rich clusters, *Mon. Not. R. Astron. Soc.* **452**, 343 (2015).
- [67] K. Osato, M. Shirasaki, and N. Yoshida, Impact of baryonic processes on weak-lensing cosmology: Power spectrum, nonlocal statistics, and parameter bias, *Astrophys. J.* **806**, 186 (2015).
- [68] G. Hinshaw *et al.*, Nine-year Wilkinson Microwave Anisotropy Probe (WMAP) observations: Cosmological parameter results, *Astrophys. J. Suppl. Ser.* **208**, 19 (2013).
- [69] P. A. R. Ade *et al.* (Planck Collaboration), Planck 2015 results. XIII. Cosmological parameters, [arXiv:1502.01589](https://arxiv.org/abs/1502.01589).
- [70] Y. S. Song, W. Hu, and I. Sawicki, Large scale structure of  $f(R)$  gravity, *Phys. Rev. D* **75**, 044004 (2007).
- [71] B. Li, G.-B. Zhao, R. Teyssier, and K. Koyama, ECOSMOG: an Efficient COde for Simulating MOdified Gravity, *J. Cosmol. Astropart. Phys.* **1** (2012) 051.
- [72] A. Lewis and S. Bridle, Cosmological parameters from CMB and other data: A Monte Carlo approach, *Phys. Rev. D* **66**, 103511 (2002).
- [73] Y. Li and W. Hu, Chameleon halo modeling in  $f(R)$  gravity, *Phys. Rev. D* **84**, 084033 (2011).
- [74] <http://www.dirac.ac.uk>.